Supporting Information

Selective Conversion of Acetone to Mesitylene over Tantalum Phosphate Catalysts

Zhiyi Wu, Jian Zhang, Zerui Su, Shiyao Lu, Jianbin Huang, Yehao Liang, Tianwei Tan,* and Feng-Shou Xiao*

Beijing Advanced Innovation Center for Soft Matter, Science and Engineering, Beijing Key Laboratory of Bioprocess, National Energy R&D Center for Biorefinery, College of Life Science and Technology
Beijing University of Chemical Technology
15 BeiSanhuan East Road, ChaoYang District, Beijing, China
E-mail: fsxiao@zju.edu.cn (F.-S. Xiao); twtan@mail.buct.edu.cn (T. Tan)

EXPERIMRNTAL SECTION

Catalyst preparation

Acetone (AR), ethanol (GC), H_3PO_4 (85*wt*%), cetyltrimethylammonium bromide (AR) were purchased from Sino-Pharm Chemical Reagent Co., Ltd. Tantalum (V) ethoxide (99.999% metal basis), mesitylene (AR) were bought from Alfa Aesar Chemical Co., Ltd. Tartaric acid (AR), Al_2O_3 (AR), TiO_2 (AR), ZrO_2 (AR), $TaCl_5$ (AR), and ethanol (AR) were bought from Aladdin Chemical Co., Ltd. 1-ethyl-3-methylimidazolium bromide was obtained from Adamas Reagent Co., Ltd.

Synthesis of Ta_2O_5, TaPO, and Ta_2O_5-HS samples. The synthesis of TaPO was similar to the method for the synthesis of NbPO according to literature.[1,2] Firstly, tantalum tartrate solution was prepared by dissolving 4.94 g of tartaric acid into a tantalum (V) ethoxide alcohol solution (12 mmol of tantalum (V) ethoxide in 50 mL of ethanol). A light-yellow colloid was obtained by heating the above solution at 80 °C. All the ethanol was evaporated by kept stirring at 80 °C for another 4 h. After cooling the colloid to room temperature, 24 mL of H_2O was added under stirring to obtain a tantalum tartrate solution (0.5 mol/L). For the synthesis of TaPO samples, 20 mL of the as-obtained tantalum tartrate solution (0.5 mol/L) was mixed with 0.65 g of H_3PO_4 and 20 mL of H_2O. A cetyltrimethylammonium bromide solution (1 g of cetyltrimethylammonium bromide in 15 mL of H_2O) was dropped into the mixed solution. The obtained suspension was kept stirring at 35 °C for 1 h, transferred into an autoclave and hydrothermally treated at 160 °C for 24 h. The solid was separated by filtrating, washing thoroughly with a large amount of water, and drying at 50 °C. The TaPO sample was obtained by calcining the solid at 550 °C for 4 h in air. The P/Ta (molar ratio of phosphorus to tantalum element) in the TaPO samples were controlled by adjusting the amount of H_3PO_4 in the synthesis gel. As a result, the samples designated as Ta_2O_5, TaPO-0.5, TaPO-1, TaPO-2, and TaPO-3 were synthesized by controlling the added amount of H_3PO_4 at 0 g, 0.65 g, 1.30 g, 2.60 g, and 3.90 g in the starting systems.

Furthermore, we have also synthesized Ta_2O_5 with higher surface area (Ta_2O_5-HS). Typically, 3.183 g of $TaCl_5$ was dispersed in 137 ml of ethanol, followed by addition of 3.418 g of 1-ethyl-3-methylimidazolium bromide and 6.836 g of H_2O. The mixture was kept stirring for 1 h and hydrothermal treated at 200 °C for 2 d. The solid was obtained by centrifugation, washing with water and methanol, and drying at 80 °C. Ta_2O_5-HS was obtained by calcining the solid at 400 °C for 3 h.

Synthesis of Pt/Al_2O_3 sample. The Pt/Al_2O_3 sample with 5 *wt*% Pt loading was synthesized *via* incipient wetness impregnation method. H_2PtCl_6 aqueous solution (AR, HWRK chemical Co. Ltd) was utilized as the precursor. After vaporing water at 80 °C, calcining at 400 °C for 4 h, the Pt/Al_2O_3 sample was obtained by reducing the solid at 300 °C for 2 h in H_2.

Catalytic conversion of acetone to mesitylene. The catalytic conversion of acetone to mesitylene was performed on a fixed bed reactor with an inner diameter of 10 mm. The catalysts were pressured, crushed, sieved into 40-60 mesh, and diluted with quartz (40-60 mesh) in the volume ratio of 1/1. The catalysts were localized in the middle part of the reactor (400 mm length, heated with a stove, a k-type thermocouple was connected with the catalysts to detect the actual reaction temperature) and pretreated at 400 °C for 2 h in N_2. The reaction was performed with reaction pressure at 1 atm and WHSV at 1.45 h^{-1}. Acetone was introduced with flowing N_2 (saturated at 0 °C, 9.3 vol%) and N_2 flow rate was controlled by a mass flow controller. The productive gas was analyzed online by a chromatograph equipped with FID detector equipped a HP-5 column. External standard method was used to quantify the unreacted acetone and the products. The line between the reactor and the chromatograph was heated to at least 200 °C to make sure that no product is condensed in the line. The acetone conversion, product selectivities, and carbon mass balance were calculated basing on the following equations:

$$\text{acetone conversion} = \frac{V_{\text{acetone outlet flow rate}}}{V_{\text{acetone inlet flow rate}}} \times 100\%,$$

$$\text{selectivity to product i} = \frac{n_i \times V_i}{n_{\text{acetone}} \times V_{\text{acetone inlet flow rate}}} \times 100\%,$$

$$\text{carbon mass balance} = \frac{\Sigma n_i \times V_i}{n_{acetone} \times V_{acetone\ inlet\ flow\ rate}} \times 100\%,$$

where i, n_i, and V_i mean acetone or the products, the carbon number in the acetone or product molecules, and the molar flow rate of the acetone or products.

Recyclable tests. The recyclable tests were also performed on the same reactor for the conversion of acetone to mesitylene. After catalyzing the conversion of acetone for 1 h, the catalyst was calcined in flowing O_2 (30 mL/min) at 400 °C for 2 h to remove the oligomers/coke, and cooled to 200 °C in N_2 for the next run.

Catalytic hydrogenation of mesitylene. The catalytic hydrogenation of mesitylene was performed on an autoclave reactor. As a typical run, 5 mmol of mesitylene, 100 mg of 5% Pt/Al_2O_3 catalyst, and 22 g of dodecane were mixture in the autoclave. The autoclave was sealed, purged with H_2 for 5 times, and charged with 4 MPa of H_2, the autoclave was heated to 220 °C and maintained for 4 h. After reaction the autoclave was cooled with cold water bath, a certain amount of bromobenzene (internal standard for GC analysis) was added into the reaction mixture after removing the catalyst by centrifugation. The unreacted substate and products were analyzed on a gas chromatograph, the products were also confirmed by GC-MS analysis.

Kinetic studies. The kinetic studies were performed on the same fixed bed reactor for the catalytic conversion of acetone to mesitylene. The reaction conditions are also similar except the WHSV at 9.5-16.5 h^{-1} and the acetone pressure were controlled at 1.04-3.11 kPa. The reaction temperature was 200 °C. The productive gas was analyzed online by a chromatograph equipped with FID detector. The line between the reactor and the chromatograph was heated to at least 200 °C to make sure that no product is condensed in the line.

Catalytic conversion of the mixture of aceotone-d_6 and mesityl oxide/acetone-d_6 and mesitylene. The catalytic conversions of the mixture of aceotone-d_6 and mesityl oxide/acetone-d_6 and mesitylene were displayed on the same reactor for the conversion of acetone to mesitylene. The reaction conditions are also similar except replacing acetone with the mixture of aceotone-d_6 and mesityl oxide/acetone-d_6 and

mesitylene. The liquid mixture was injected by a pump (0.6 mL/h) and vaporized before contacting with the catalyst. The mass of catalyst was 0.32 g and the reaction temperature was 200 °C. The products were collected with dodecane (cooled with ice bath), and analyzed with an Agilent 7890B-5977A GC-MS apparatus.

Catalyst Characterization

X-ray diffraction (XRD) patterns were measured on a Bruker AXS D8 FOCUS diffractometer with Cu Kα radiation (λ=1.54 Å). Nitrogen sorption isotherms were measured using a Micromeritics ASAP 2460 system. The samples were pretreated at 120 °C overnight under vacuum overnight. Bulk P/Ta values were determined by inductively coupled plasma (ICP) analysis (Perkin-Elmer 3300DV). Transmission electron microscopy (TEM), scanning transmission electron microscopy (STEM), and energy dispersive spectrometer (EDS) analysis were performed on a JEOL JEM-2100F electron microscope with an acceleration voltage of 200 kV. XPS experiments were carried out using a Kratos Axis Ultra DLD photoelectron instrument using a monochromatic Al Kα (1486.6 eV) X-ray source. The binding energy (BE) values were calibrated using the C1s peak at 284.9 eV. Metal contents were determined by inductively coupled plasma (ICP) analysis (Perkin-Elmer 2100). Solid state ^{31}P-NMR spectra were recorded on a Bruker AV300 spectrometer, the ^{31}P chemical shifts were externally referenced to 85% H_3PO_4. Thermal gravimetric analysis (TGA) experiments were performed on a SDT Q600 V8.2 Build100 thermogravimetric analyzer in air flow with a ramp rate of 10 °C/min. Pyridine adsorption FT-IR spectra were performed on a Bruker Tensor 27 FT-IR spectrometer. The samples were pretreated at 400 °C for 1 h, adsorption of pyridine at 50 °C, and vacuum treated at 200 °C for each test. Temperature programmed desorption of NH_3 (NH_3-TPD) were performed on a Micromeritics AutoChem 2920 chemisorption analyzer. The samples were pretreated in flowing Ar at 400 °C for 1 h and subsequent adsorption of NH_3 at 100 °C for 1 h. After sweeping at 120 °C for another 1 h, the samples were heated to 800 °C in He flow with a ramp rate of 10 °C/min.

Computational methods. The present first principle calculations are performed by Vienna Ab initio Simulation Package (VASP)[3] with the projector augmented wave

(PAW) method[4] based on density functional theory. The exchange-functional is treated with the generalized gradient approximation (GGA) of Perdew-Burke-Ernzerhof (PBE) functional.[3] The energy cutoff for the plane wave basis expansion has been set to 400 eV for convergence criterion of geometry relaxation. For bulk structure, a 4×4×4 Monkhorst and Pack k-point sampling was employed in our calculations.[5] The role of van der Waals (VDW) force is also considered in the calculation. The self-consistent calculations apply a convergence energy threshold of 10^{-6} eV. The equilibrium lattice constants are optimized with maximum stress on each atom within 0.05 eV/Å. The vacuum spacing in a direction perpendicular to the plane of the catalyst is at least 10 Å.

The Brillouin zone integration is performed using 3×3×1 Monkhorst and Pack k-point sampling for surface and interface.

In addition, spin polarizations are also considered in our calculations. The Hubbard U (DFT+U) corrections for 3d transition metal by setting according to the literature.[6]

The free energy was calculated using the equation[7]:

$$G = E + ZPE - TS$$

where G, E, ZPE and TS represents the free energy, total energy from DFT calculations, zero-point energy and entropic contributions (T was set to be 300 K), respectively. ZPE could be derived after frequency calculation by[8]:

$$ZPE = \frac{1}{2}\sum h\nu_i$$

And the TS values of adsorbed species are calculated after obtaining the vibrational frequencies[9]:

$$TS_\nu = k_B T\left[\sum\nolimits_K \ln\left(\frac{1}{1-e^{-h\nu/k_B T}}\right) + \sum\nolimits_K \frac{h\nu}{k_B T}\frac{1}{(e^{h\nu/k_B T}-1)} + 1\right]$$

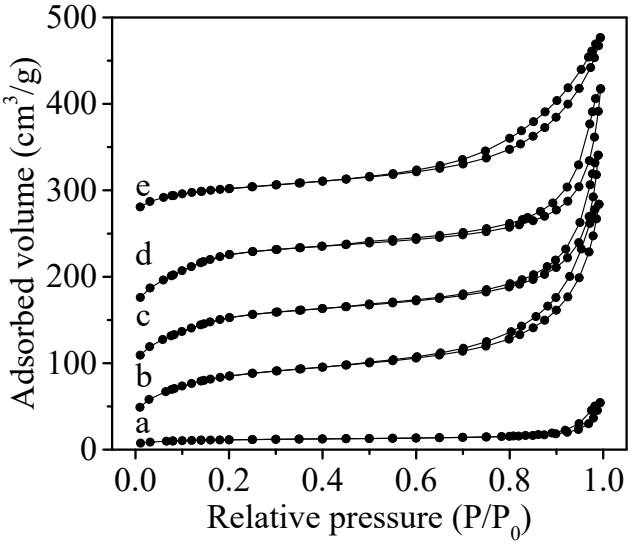

Figure S1. N_2-sorption isotherms of the (a) Ta_2O_5, (b) TaPO-0.5, (c) TaPO-1, (d) TaPO-2, and (e) TaPO-3 samples.

Note: N_2-sorption isotherms were displayed to investigate the porosity on the TaPO samples (Figure S1). The Ta_2O_5 sample shows a gradual step in the regions at $P/P_0 < 0.2$ and $0.8 < P/P_0 < 1.0$, indicating the presence of mesopores. Correspondingly, the BET surface area and pore volume are 36.5 m^2/g and 0.084 cm^3/g, respectively (Table S1). The introduction of phosphate in the synthesis gel is beneficial for the enhancement of the mesoporosity in the TaPO samples. For example, the BET surface area and pore volume of TaPO-0.5 are 268.8 m^2/g and 0.43 cm^3/g, respectively (Table S1). Further increasing of phosphate in the synthesis gel firstly leads to the increase of the BET surface area and pore volume, then the decrease of the BET surface area and pore volume (Figure S1 and Table S1). The BET surface areas and pore volumes of TaPO-1, TaPO-2, and TaPO-3 samples are 314.1, 354.5, and 174.3 m^2/g and 0.43, 0.46, and 0.35 cm^3/g, respectively (Table S1).

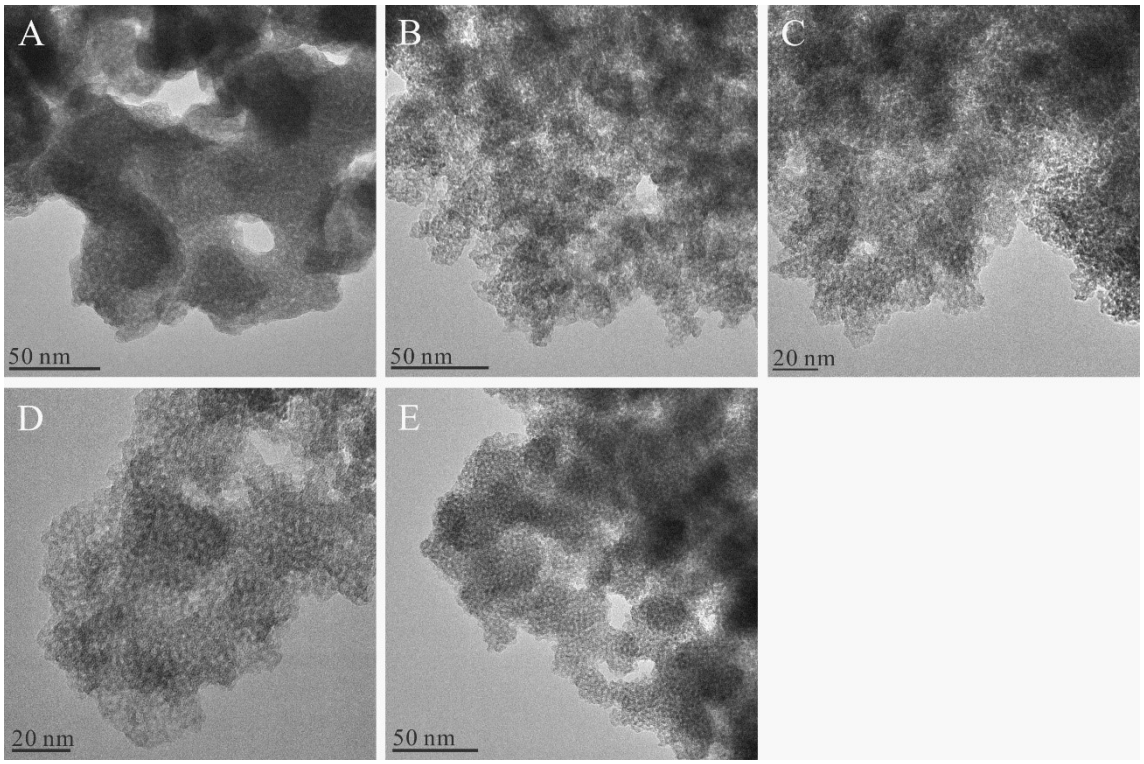

Figure S2. TEM images of the (A) Ta_2O_5, (B) TaPO-0.5, (C) TaPO-1, (D) TaPO-2, and (E) TaPO-3 samples.

Note: All the samples exhibit abundant small mesopores with size at about 2 nm and many intracrystal mesopores with size at about 10~25 nm.

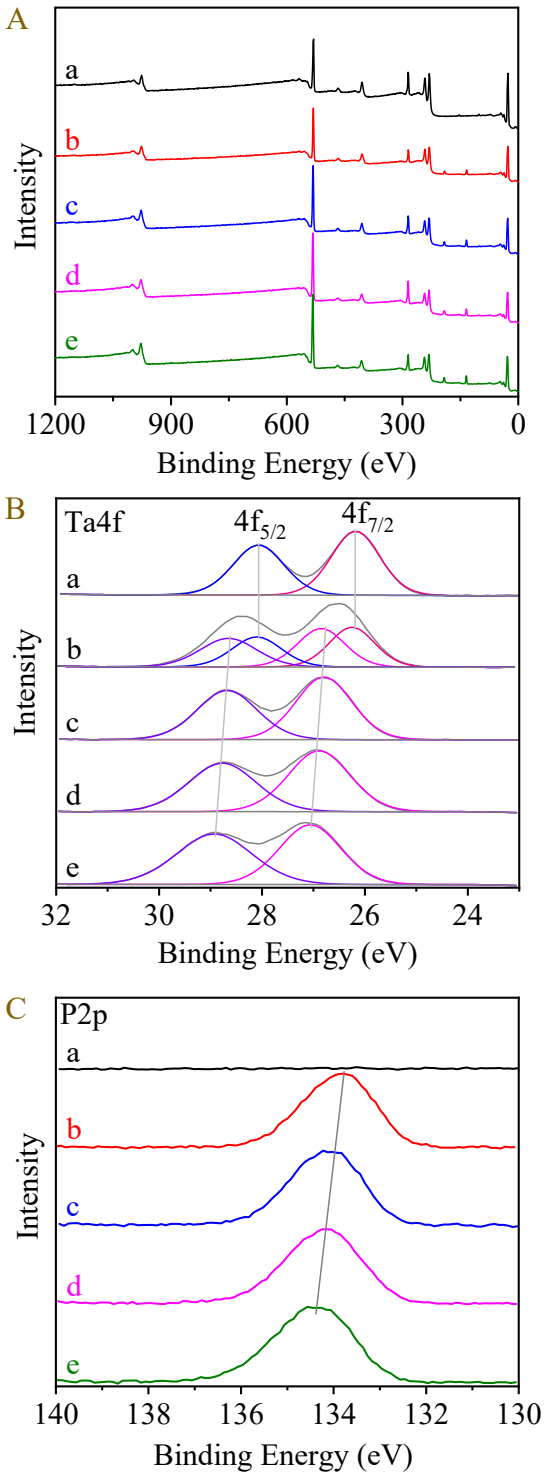

Figure S3. (A) Wide spectrum, (B) Ta4f, and (C) P2p XPS spectra of the (a) Ta_2O_5, (b) TaPO-0.5, (c) TaPO-1, (d) TaPO-2, and (e) TaPO-3 samples.

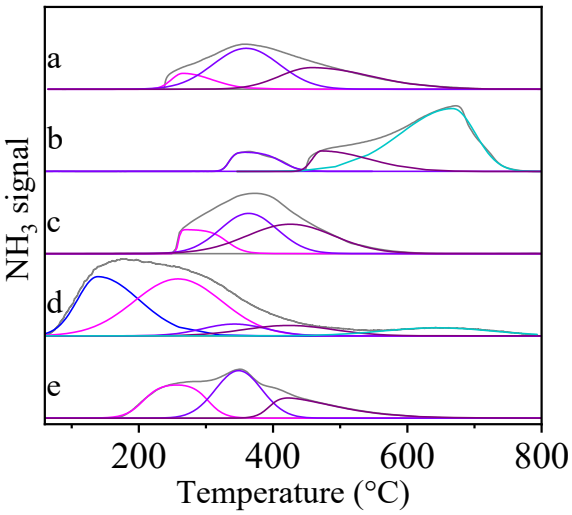

Figure S4. Temperature-programmed-desorption of NH_3 (NH_3-TPD) profiles over (a) TaPO-0.5, (b) TaPO-1, (c) TaPO-2, (d) TaPO-3, and (e) Ta_2O_5 samples. The peaks associated with weak (A_w), medium (A_M), medium-strong (A_{MS}), strong (A_S), and ultra-strong (A_{US}) acidic sites were colored by blue, pink, violet, purple, and green, respectively.

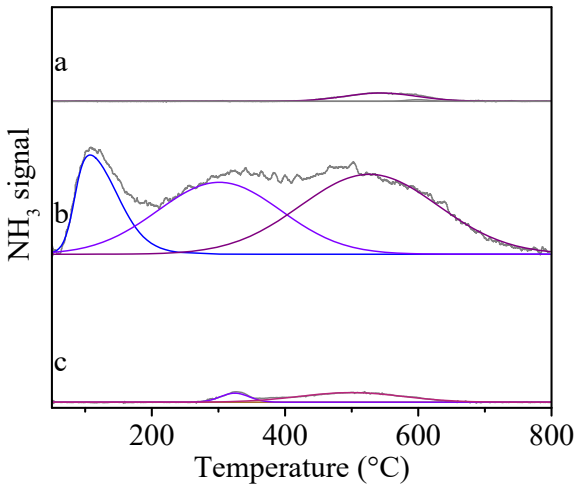

Figure S5. NH_3-TPD profile of (a) TiO_2, (b) Al_2O_3, and (c) ZrO_2 samples.

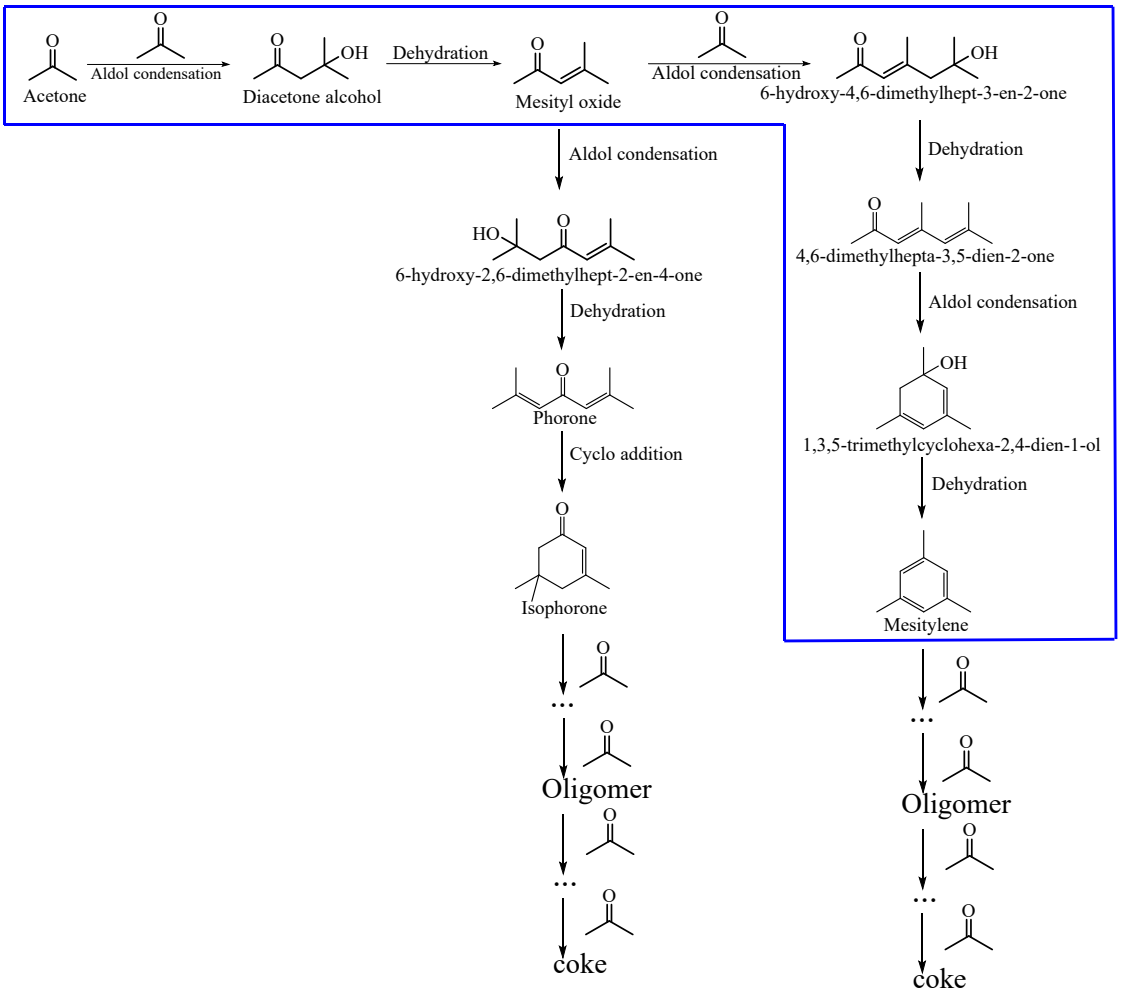

Figure S6. Reaction pathway during the catalytic conversion of acetone. The blue rectangle highlights the pathway for the production of mesitylene from acetone.

Note: The catalytic conversion of acetone to mesitylene consists of sequential aldol condensation reactions and dehydration reactions. The reaction is initiated by the intramolecular aldol condensation of acetone, catalyzing by acid or basic sites. The as-formed diacetone alcohol underwent dehydration reaction to form mesityl oxide. The mesityl oxide would react with another acetone molecule to form two kinds of products: 6-hydroxy-2,6-dimethylhept-2-en-4-one and 6-hydroxy-4,6-dimethylhept-3-en-2-one. The former molecule underwent dehydration reaction to form phorone, which sequentially underwent cycloaddition to isophorone. The latter molecule underwent dehydration reaction to form 4,6-dimethylheptan-3,5-dien-2-one, which sequentially underwent intermolecular aldol condensation reaction to 1,3,5-

trimethylcyclohexa-2,4-dien-1-ol. 1,3,5-trimethylcyclohexa-2,4-dien-1-ol would quickly dehydration to form mesitylene. Isophorone and mesitylene might further react with several acetone molecules to form oligomers/coke.

Furthermore, some side products such as C1-C4 alkanes might also be formed: the catalytic reforming might produce isobutene (C4) and acetic acid, and the catalytic reforming of acetone might produce methane (C1). The catalytic dehydration of acetone might produce propylene (C3), and the cracking of propylene might produce C1 and C2 products.

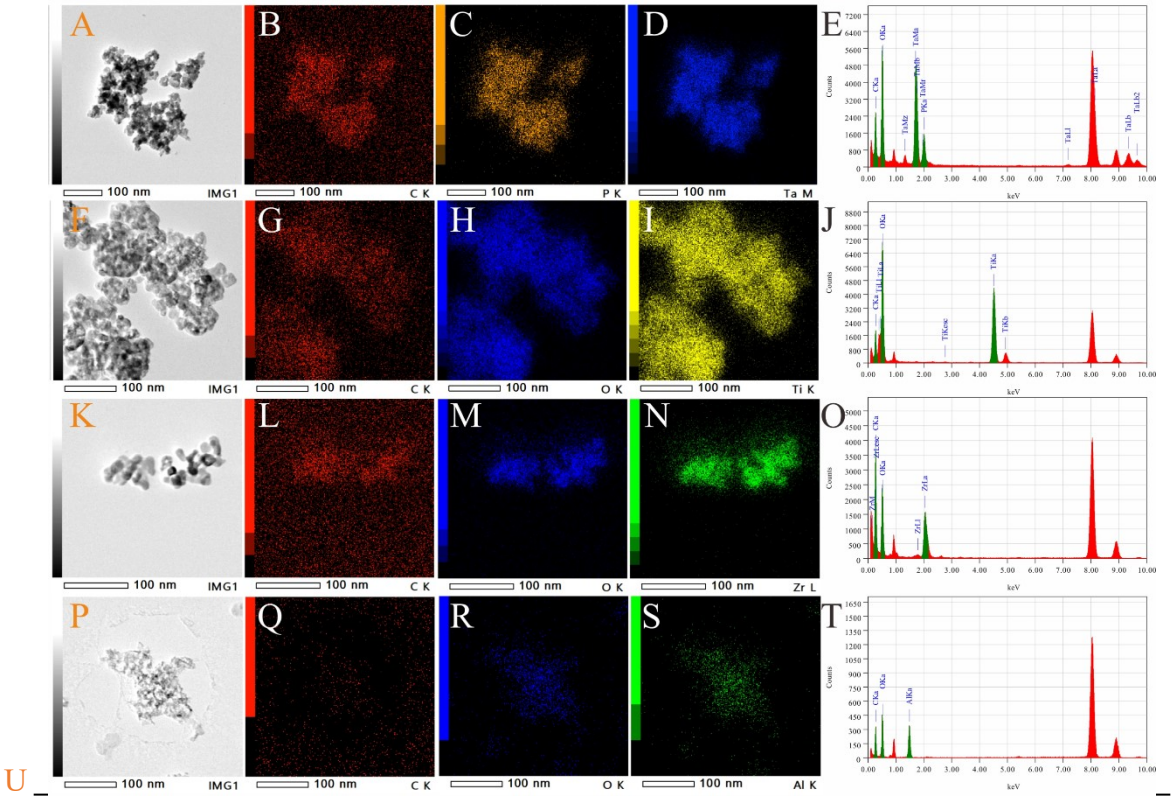

U

Sample	Element content (*wt*%)			
TaPO-1	18.69% C	21.78% O	6.01% P	53.52% Ta
TiO_2	21.03% C	36.49% O	42.49% Ti	
ZrO_2	48.35% C	16.50% O	35.15% Zr	
Al_2O_3	41.47% C	39.35% O	19.18% Al	

Figure S7. (A, F, K, and P) STEM images, (B-D, G-I, L-N, and Q-S) the corresponding elemental map, and (E, J, O, and T) EDS analysis of the spent (A-E) TaPO-1, (F-J) TiO_2, (K-O) ZrO_2, and (P-T) Al_2O_3 samples. (U) The elemental content of the above samples basing on the EDS analysis.

Note: The formation of oligomers/coke were also supported by the TEM technique. The spent TaPO-1, TiO_2, ZrO_2, and Al_2O_3 samples were treated under vacuum to remove the physically adsorbed acetone and other products with low molecular weight. The obtained samples were characterized by STEM images and elemental mapping technique (Figure S7A-T). It can be clearly observed that the locations of

carbon element are the same as other elements in all the samples, indicating the formation of oligomer/coke in all the catalysts. The element contents were calculated basing on the EDS analysis. The spent TaPO-1 samples exhibited carbon element content at 18.69%, while the TiO_2, Al_2O_3, and ZrO_2 samples exhibited carbon element content at 21.03%, 48.35%, and 41.47%, separately. The relative higher carbon amounts in the TiO_2, Al_2O_3, and ZrO_2 samples confirm again that oligomers/coke are the major side products for these catalysts during the catalytic conversion of acetone.

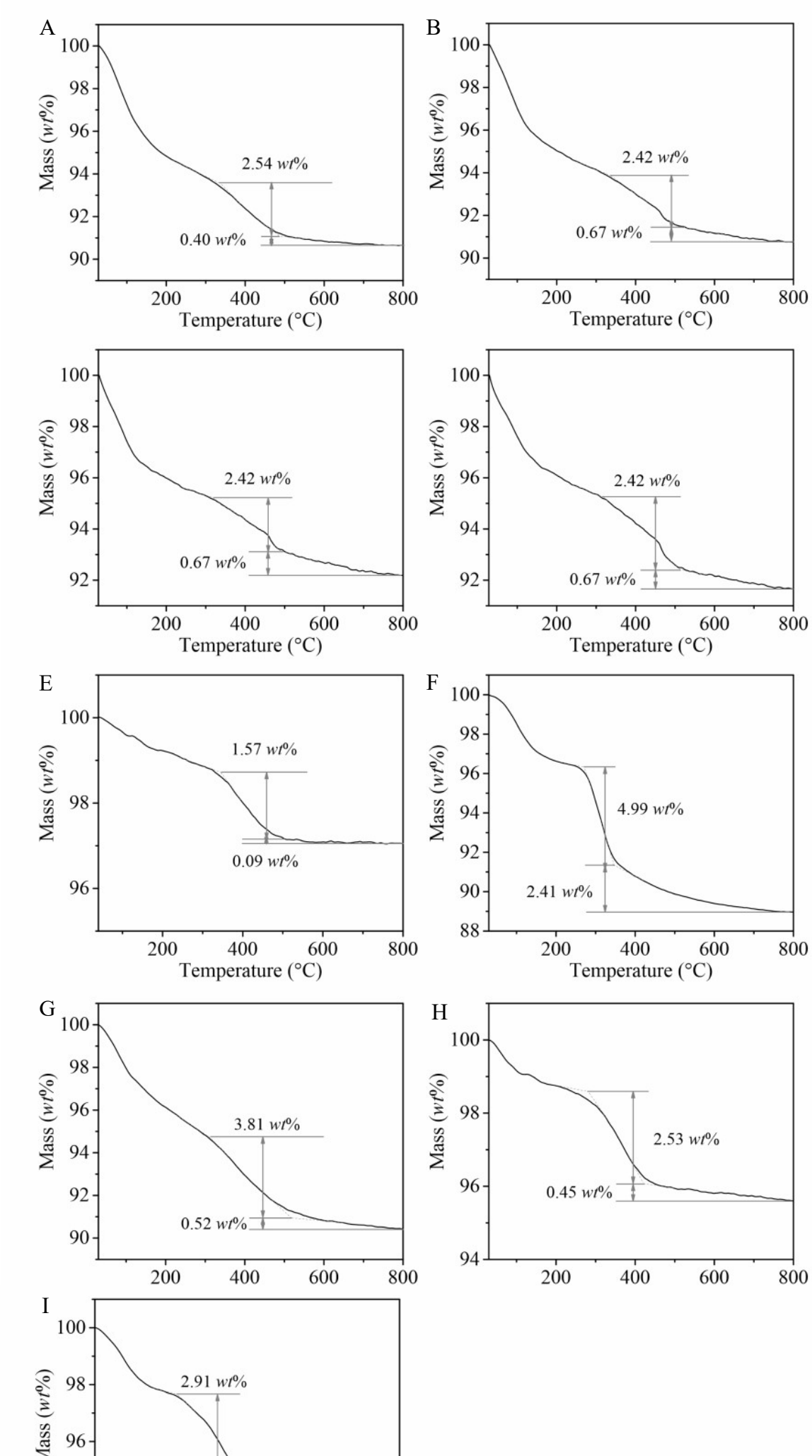
A
Mass (wt%)
Temperature (°C)
2.54 wt%
0.40 wt%
B
2.42 wt%
0.67 wt%
2.42 wt%
0.67 wt%
2.42 wt%
0.67 wt%
E
1.57 wt%
0.09 wt%
F
4.99 wt%
2.41 wt%
G
3.81 wt%
0.52 wt%
H
2.53 wt%
0.45 wt%
I
2.91 wt%

Figure S8. Thermogravimetric (TG) analysis of the spent (A) TaPO-0.5, (B) TaPO-1, (C) TaPO-2, (D) TaPO-3, (E) Ta_2O_5, (F) TiO_2, (G) Al_2O_3, (H) ZrO_2, and (I) MgO samples.

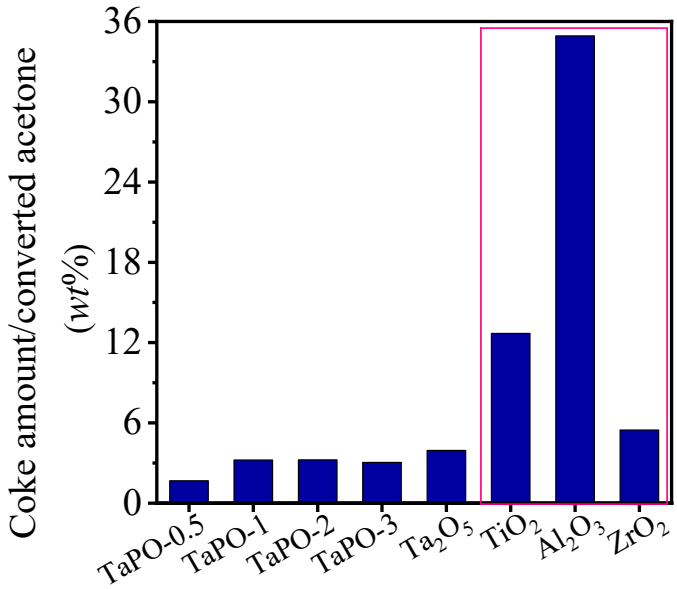

Figure S9. Coke amount/converted acetone over these catalysts after reaction for 1 h. Reaction conditions: 0.3 g of catalyst, 9.3 vol % acetone in N_2, WHSV at 1.45 h^{-1}, 200 °C, reaction for 1 h. The catalysts were pretreated at 400 °C for 2 h in N_2. The red rectangle in Figure S9 highlights the values of coke amount/converted acetone higher than 5%.

Note: Because oligomers/coke cannot be precisely detected by on-line chromatography, we performed thermogravimetric (TG) analysis (Figure S8). We calculated the values of oligomers/coke with converted acetone (coke amount/ converted acetone) to study the oligomers/coke formation during the reaction processes, which are 1.7, 3.2, 3.2, 3.1, 3.9, 12.7, 34.9, and 5.5 *wt*% for TaPO-0.5, TaPO-1, TaPO-2, TaPO-3, Ta_2O_5, TiO_2, Al_2O_3, and ZrO_2, respectively (Figure S9). Notably, the catalysts with lower selectivities to mesitylene all exhibited coke amount/converted acetone higher than 5.0% (red rectangle in Figure S9), while all the TaPO samples with relatively high mesitylene selectivity have coke amount/converted acetone lower than 4.0%. According to these results, it is suggested that the major side products were oligomers/coke.

A

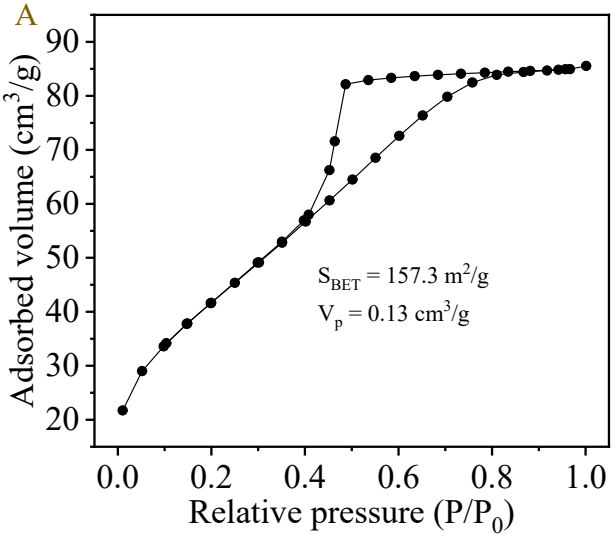

B

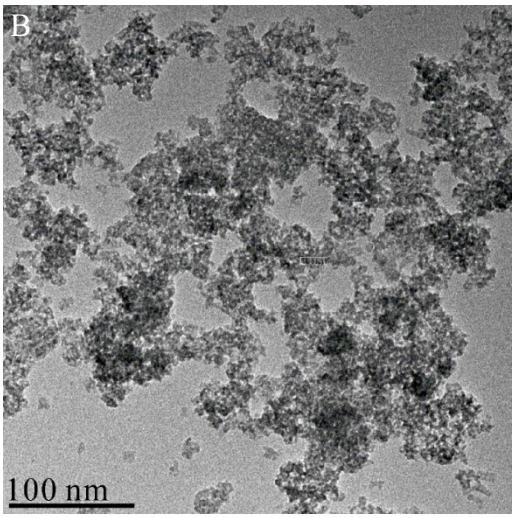

C

Acetone conversion (%)	Selectivity (%)			Carbon balance (%)
	Mesityl oxide	Mesitylene	Oligomer/coke	
47.5	17.7	31.9	50.4	76.0

Figure S10. (A) N_2-sorption isotherms, (B) TEM image, and (C) Catalytic results in the conversion of acetone of the Ta_2O_5-HS sample. Reaction conditions: 0.3 g of catalyst, 9.3 vol % acetone in N_2, WHSV at 1.45 h^{-1}, 200 °C, reaction for 1 h. The catalysts were pretreated at 400 °C for 2 h in N_2.

Note: The surface area of the Ta_2O_5 catalyst might affect the catalytic performance of the catalyst. We have made a Ta_2O_5 sample (designated as Ta_2O_5-HS) with S_{BET} and V_p at 157.3 m^2/g and 0.13 cm^3/g by hydrothermal treating 3.183 g of $TaCl_5$ in a mixed solution (3.418 g of 1-ethyl-3-methylimidazolium bromide, 6.836 g of H_2O, and 137 ml of ethanol) at 200 °C. TEM image and N_2-sorption isotherms confirm the high surface area and mesopores in the Ta_2O_5-HS sample (Figure S10). When this catalyst was applied in the catalytic conversion of acetone to mesitylene, it was given acetone conversion and mesitylene selectivity at 47.5% and 31.9% (Figure S10C), which are even lower than those of the Ta_2O_5 with surface area < 50 m^2/g. Therefore, it is found that the catalytic performance of the Ta-containing catalysts is not sensitive to the surface area of the catalysts.

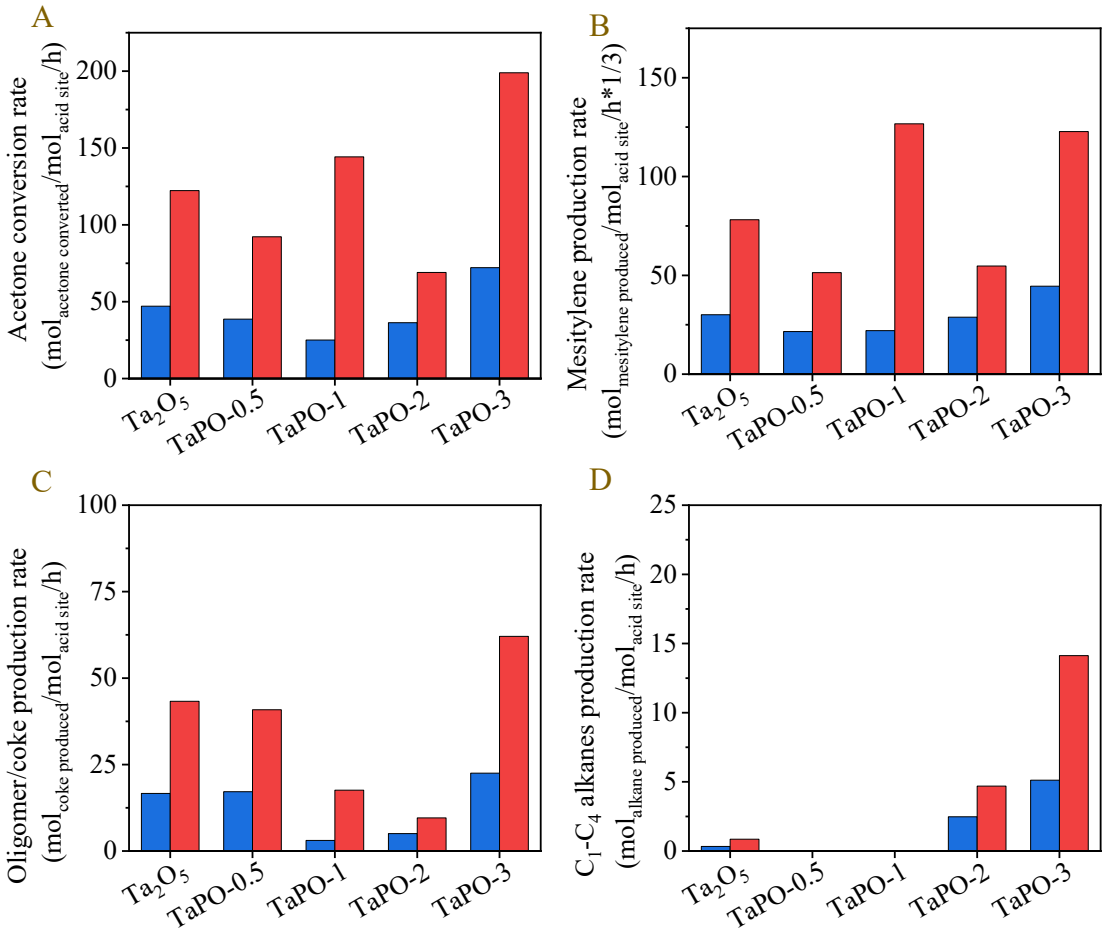

Figure S11. (A) Acetone Conversion rate, (B) Mesitylene, (C) oligomer/coke, and (D) C_1-C_4 production rate normalized by total strong acid sites (A_{MS}+A_S+A_{us}, blue column) or strong acid sites (A_S, red column) in the catalytic conversion of acetone to mesitylene over various Ta-containing catalysts. Reaction conditions: 0.3 g of catalyst, 9.3 vol % acetone in N_2, WHSV at 1.45 h^{-1}, 200 °C, reaction for 1 h. The catalysts were pretreated at 400 °C for 2 h in N_2.

Note: Unfortunately, the normalization of the catalytic results of the TaPO catalysts by acid sites did not clearly point out the dominant active sites for the main reaction. This phenomenon might be resulted from reasons in the following: (i) Because oligomer/coke were formed in the reaction process, the number of active sites would be reduced with increasing reaction time by the coke formation; (ii) acetone as a sole substrate during the reaction, might participate in almost all steps in the

reaction, where it is difficult to distinguish the active sites for each step by simple normalization of the catalytic results with acid sites in the reaction.

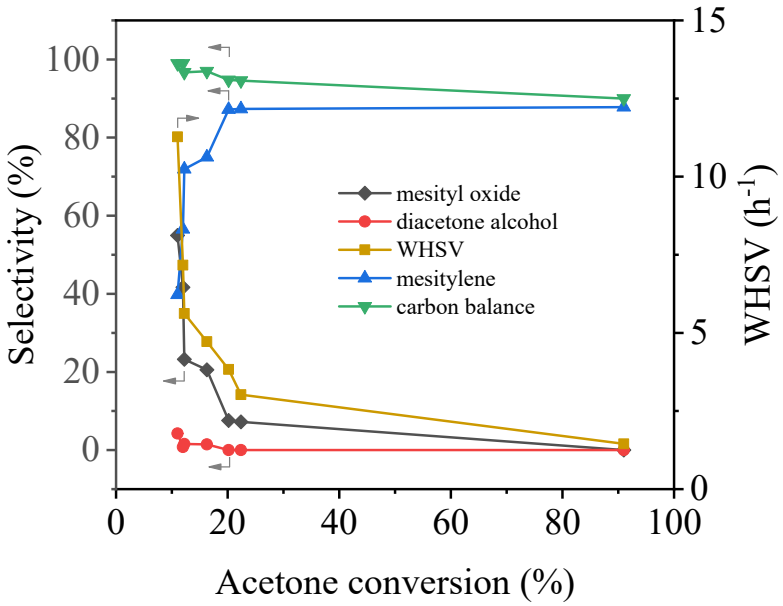

Figure S12. Products distribution as a function of acetone conversion over the TaPO-1 catalyst. Reaction conditions: WHSV at 1.45-11.3 h^{-1}, 9.3 vol % acetone in N_2, 200 °C, reaction for 1 h.

Note: the selectivity-conversion plots are quite helpful to clearly determine the reaction pathways. However, the catalytic conversion of acetone over the TaPO catalysts were performed on a fixed-bed reactor, it is difficult to achieve desired acetone conversions by changing the reaction time. Therefore, we adjusted the WHSV values in the range of 1.45-11.3 h^{-1} to achieve the selectivity-conversion plots (Figure S12). At 11.0% acetone conversion (WHSV at 11.3 h^{-1}), the selectivity to mesityl oxide, diacetone alcohol, and mesitylene were 55.0%, 4.2%, and 39.8%, respectively. In this case, the carbon balance was 99.0%, only exhibiting 1.0% oligomer/coke selectivity. Decreasing WHSV led to enhanced acetone conversion, giving enhanced selectivity for mesitylene and reduced selectivities for mesityl oxide and diacetone alcohol. These results suggest that the mesitylene are produced with mesityl oxide and diacetone alcohol. Particularly, the carbon balance reduced with increasing acetone conversion, therefore it is suggested that the oligomer/coke might be derived from the oligomerization of mesityl oxide and mesitylene.

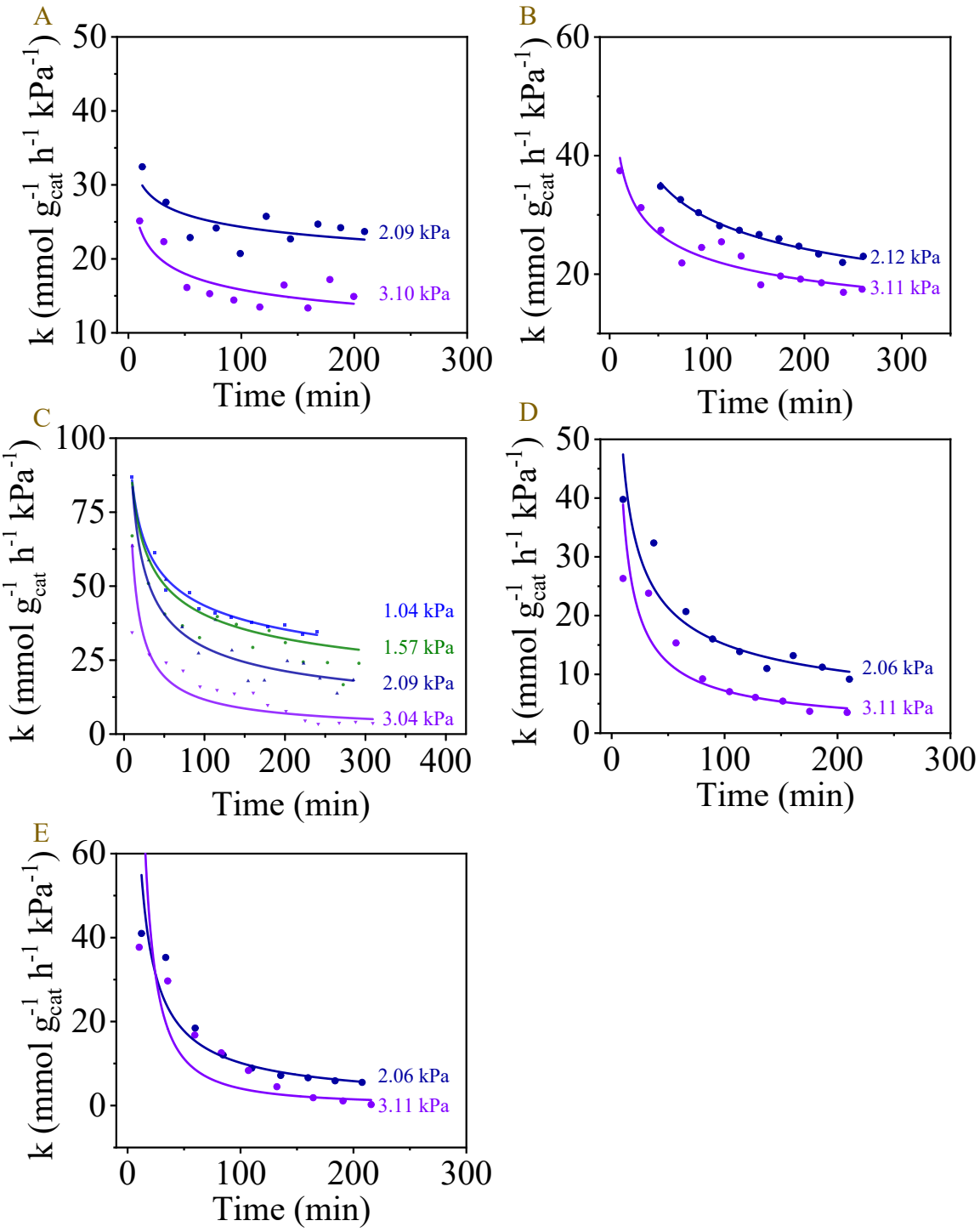

Figure S13. Reaction rate constant under different acetone pressure as a function of reaction time over (A) Ta_2O_5, (B) TaPO-0.5, (C) TaPO-1, (D) TaPO-2, and (E) TaPO-3 samples in the catalytic transformation of acetone to mesitylene. Reaction conditions: total gas flow (acetone in N_2, acetone pressure at 1.04-3.11 kPa) rate at 25-45 mL/min, WHSV at 9.5-16.5 h^{-1}, 200 °C. The catalysts were pretreated at 400 °C for 2 h in N_2.

Note: The product distribution as a function of acetone conversion should be performed to understand the catalytic performances of the TaPO catalysts. However, oligomers/coke are always formed during the entire reaction process, which would greatly influence the reaction rate and product distribution. Thus, we displayed the reaction rate and products distribution as a function of reaction time to study the relation between acetone conversion rate (k_t) and product distribution (C_9/C_6) (Figures S13-15). It can be clearly observed that the reaction rate decreased with time-on-stream for all reactions, even at low acetone conversions (Figure S10). Furthermore, it is observed that the molar ratio of mesitylene to mesityl oxide (C_9/C_6) increased linearly with reaction rate (Figures S15). It can be concluded that the formation of oligomers/coke only cover parts of the active sites, causing the deactivation along the reaction process. While the uncovered active sites remained the catalytic abilities, which would not be affected by the formation of oligomers/coke.

The reaction rate constants were calculated basing on the following equation:

$$k\ (mmol_{acetone\ converted}\ g_{cat}^{-1}\ h^{-1}\ kPa_{acetone}^{-1}) = \frac{Reaction\ rate\ (mmol_{acetone\ converted}\ g_{cat}^{-1}\ h^{-1})}{P_{acetone}\ (kPa)}$$

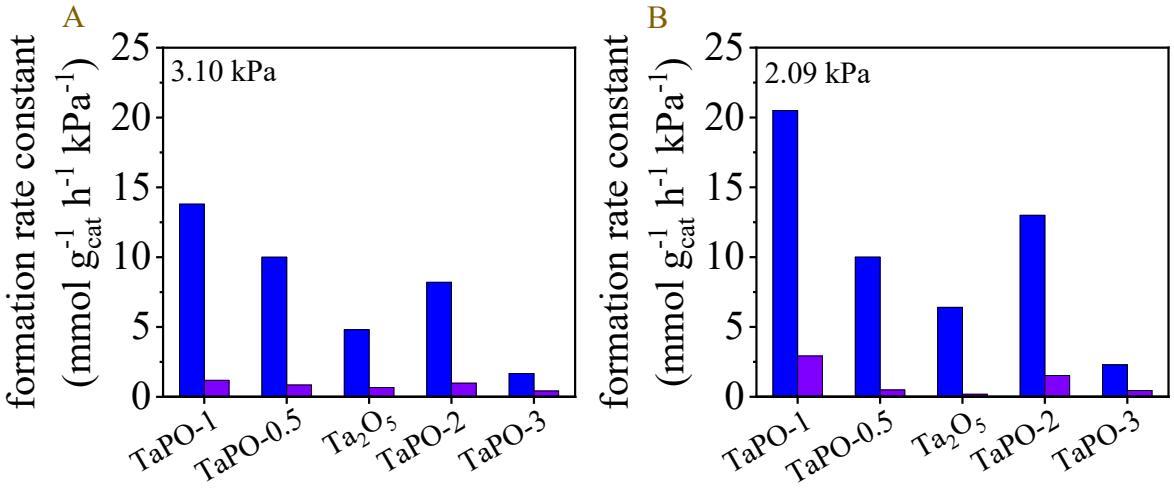

Figure S14. Formation rate of mesityl oxide (blue) and mesitylene (violet) under acetone pressure at (A) 3.10 kPa and (B) 2.09 kPa as a function of reaction time over TaPO-0.5, TaPO-1, TaPO-2, TaPO-3, and Ta_2O_5 samples in the catalytic transformation of acetone to mesitylene. Reaction conditions: total gas flow (ethanol in N_2, acetone pressure at 1.04-3.11 kPa) rate at 25-45 mL/min, WHSV at 99.5-145.0 h^{-1}, 200 °C. The catalysts were pretreated at 400 °C for 2 h in N_2. Due to technique reason, the acetone pressure in A and B are 3.04-3.11 kPa and 2.06-2.12 kPa.

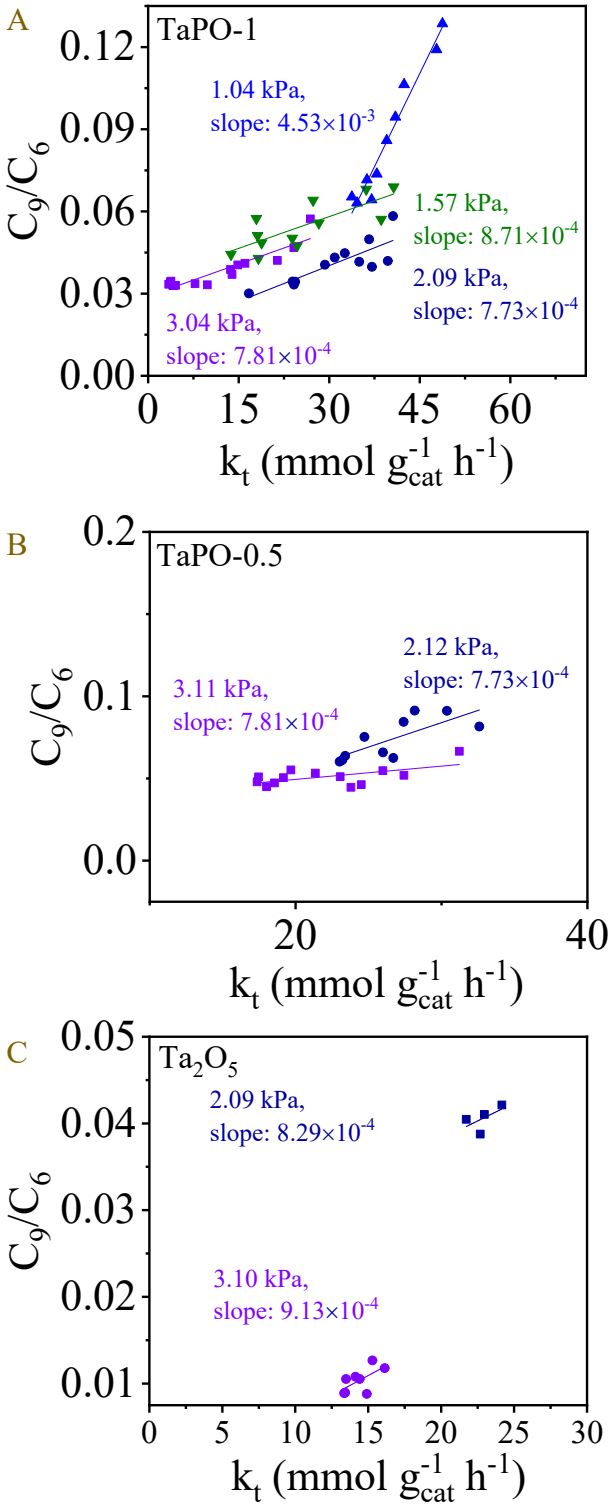

Figure S15. The ratio of formation rate of mesitylene to mesityl oxide (C_9/C_6) under different acetone pressure as a function of reaction rate constant variation over (A) TaPO-1, (B) TaPO-0.5, and (C) Ta_2O_5 samples in the catalytic transformation of acetone to mesitylene.

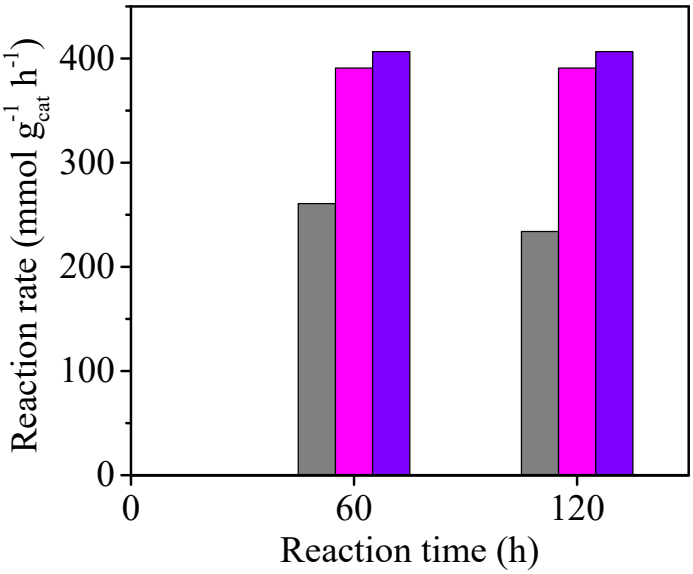

Figure S16. Reaction rate as a function of reaction time over TaPO-1 (violet), TaPO-0.5 (pink), and Ta_2O_5 (gray) samples in the catalytic dehydration of diacetone alcohol. Reaction conditions: total gas flow (diacetone alcohol in N_2, diacetone alcohol pressure at 10.1 kPa) rate at 35 mL/min, WHSV at 31.3-47.0 h^{-1}, 200 °C. The catalysts were pretreated at 400 °C for 2 h in N_2.

Note: Because the dehydrated products (diacetone alcohol, 6-hydroxy-4,6-dimethylhept-3-en-2-one, and 1,3,5-trimethylcyclohexa-2,4-dien-1-ol) were rarely detected during the reactions, it is proposed that the dehydrations proceed faster than the aldol condensations. To certify this hypothesis, the catalytic dehydration of diacetone alcohol was performed (Figure S16). At 200 °C, the Ta_2O_5, TaPO-0.5, and TaPO-1 samples all exhibited high activities in the dehydration of diacetone alcohol. After dehydration for 1 h, the Ta_2O_5, TaPO-0.5, and TaPO-1 samples displayed at 260.8, 390.9, and 406.6 mmol/g_{cat}/h, respectively, which are much higher than the rates in the aldol condensation step (Figure S13). These results indicate that the dehydration steps are much faster than the aldol condensation steps in the transformation of acetone.

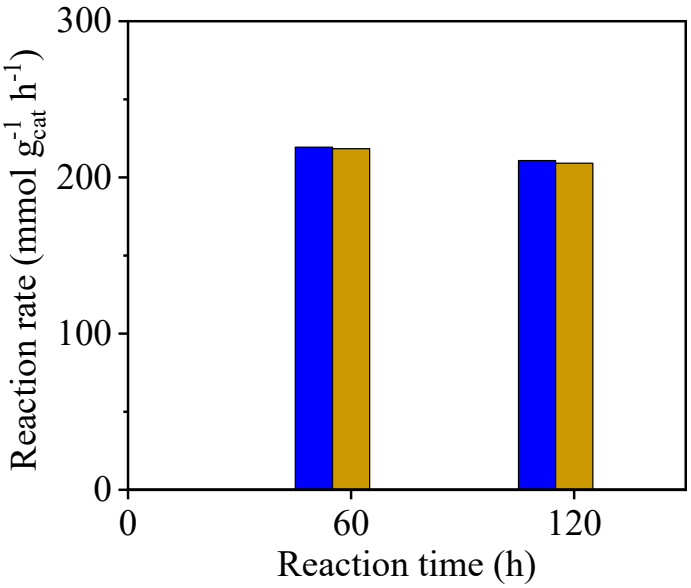

Figure S17. Reaction rate as a function of reaction time over ZrO_2 (blue) and MgO (brown) samples in the catalytic dehydration of diacetone alcohol. Reaction conditions: total gas flow (diacetone alcohol in N_2, diacetone alcohol pressure at 10.1 kPa) rate at 35 mL/min, WHSV at 24.2-25.5 h^{-1}, 200 °C. The catalysts were pretreated at 400 °C for 2 h in N_2.

Note: The dehydration steps over basic catalysts such as ZrO_2 and MgO should also studied. To certify our proposal, we performed the dehydration of diacetone alcohol at 200 °C. As shown in the above Figure, the MgO and ZrO_2 catalysts exhibited diacetone alcohol conversion rate at 219.4 and 210.8 mmol/g_{cat}/h, respectively. These values are higher than the conversion rate of acetone during the reaction, showing that the dehydration step is also not a key step over the MgO and ZrO_2 catalysts.

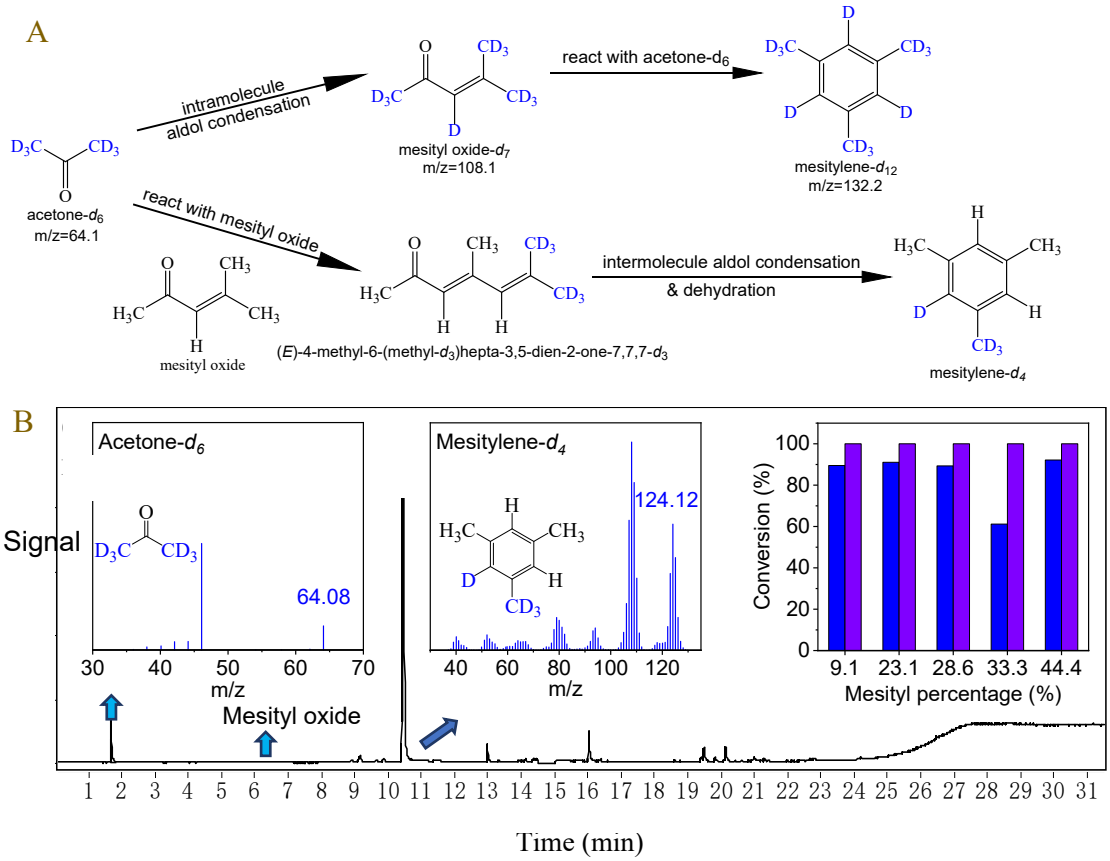

Figure S18. (A) Possible steps in the conversion of a mixture of acetone-d_6 and mesityl oxide; (B) GC-MS profile of the product over TaPO-1 catalyst in the conversion of the mixture of acetone-d_6 and mesityl oxide. Reaction conditions: 0.32 g of catalyst, mixture flow rate 0.6 ml/h, N_2 30mL/min, 200 °C, reaction for 1 h. The right insert in B was the conversion of acetone-d_6 (blue) and mesityl oxide (violet) as a function of mesityl oxide molar percentage, other inserts in B are the MS profile of acetone-d_6 and mesitylene-d_4.

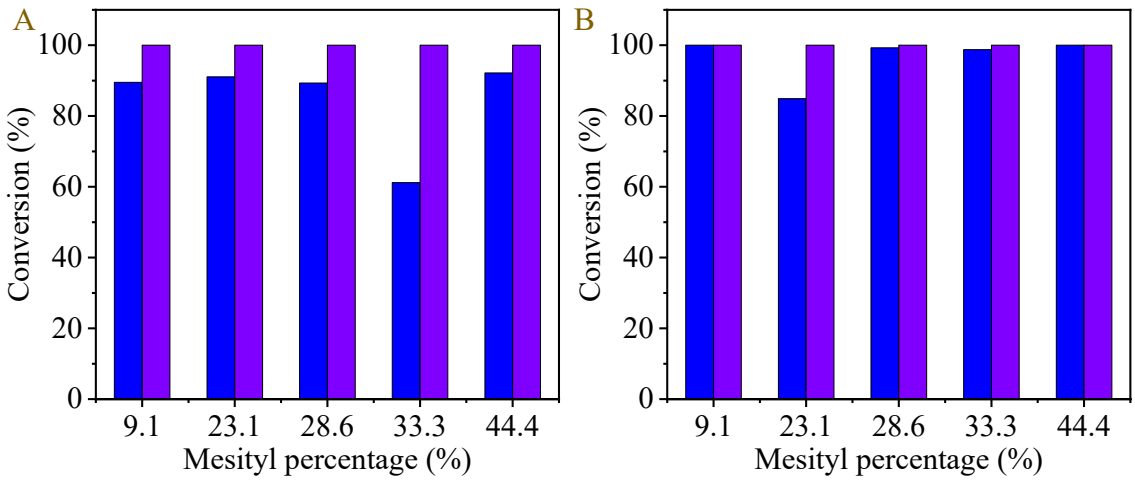

Figure S19. Conversion of acetone-d_6 (blue) and mesityl oxide (violet) as a function of mesityl oxide molar percentage over (A) Ta_2O_5 and (B) TaPO-0.5, Reaction conditions: 0.32 g of catalyst, mixture flow rate 0.6 mL/h, N_2 30mL/min, 200 °C, time-on-stream 1h.

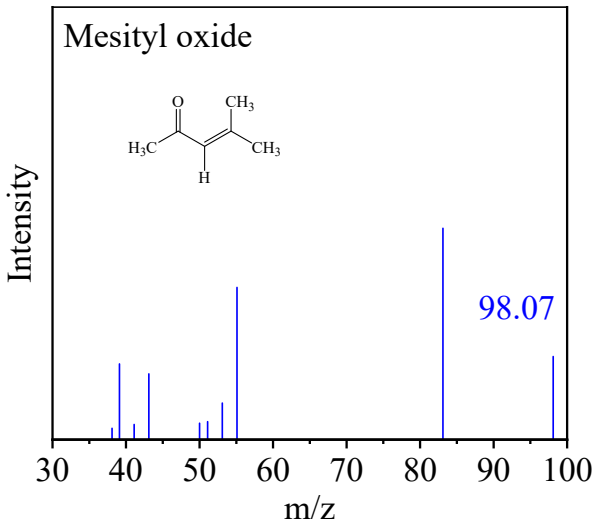

Figure S20. Mass spectrum of mesityl oxide.

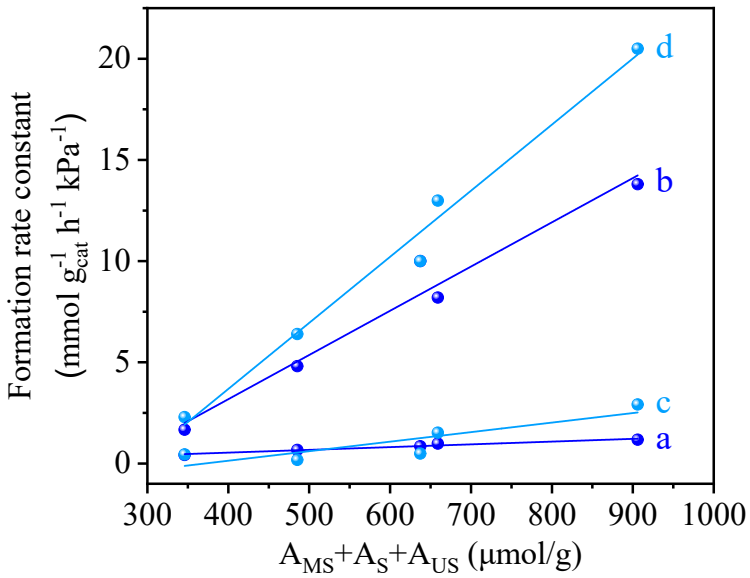

Figure S21. (a and b) Mesitylene and (b and d) mesityl oxide formation rate as a function of the total strong acid concentration (A_{MS}+ A_S+ A_{US}) with acetone pressure at (a and b) 3.10 kPa and (c and d) 2.09 kPa over the TaPO-0.5, TaPO-1, TaPO-2, TaPO-3, and Ta_2O_5 samples.

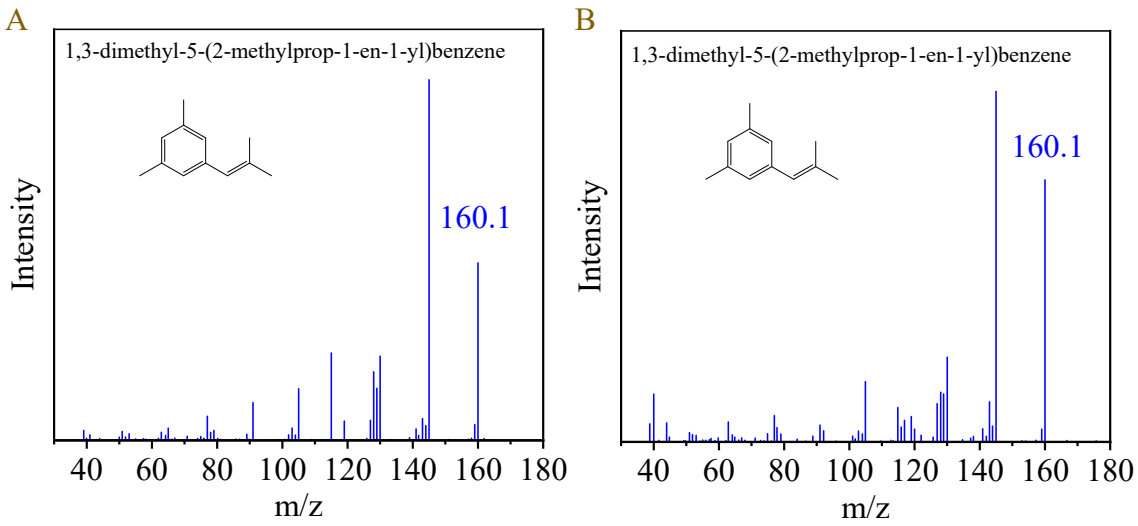

Figure S22. MS profile of (A) the major product in conversion of mesityl oxide with acetone and (B) the acetone tetramer in the catalytic conversion of acetone over the TaPO-1 catalyst.

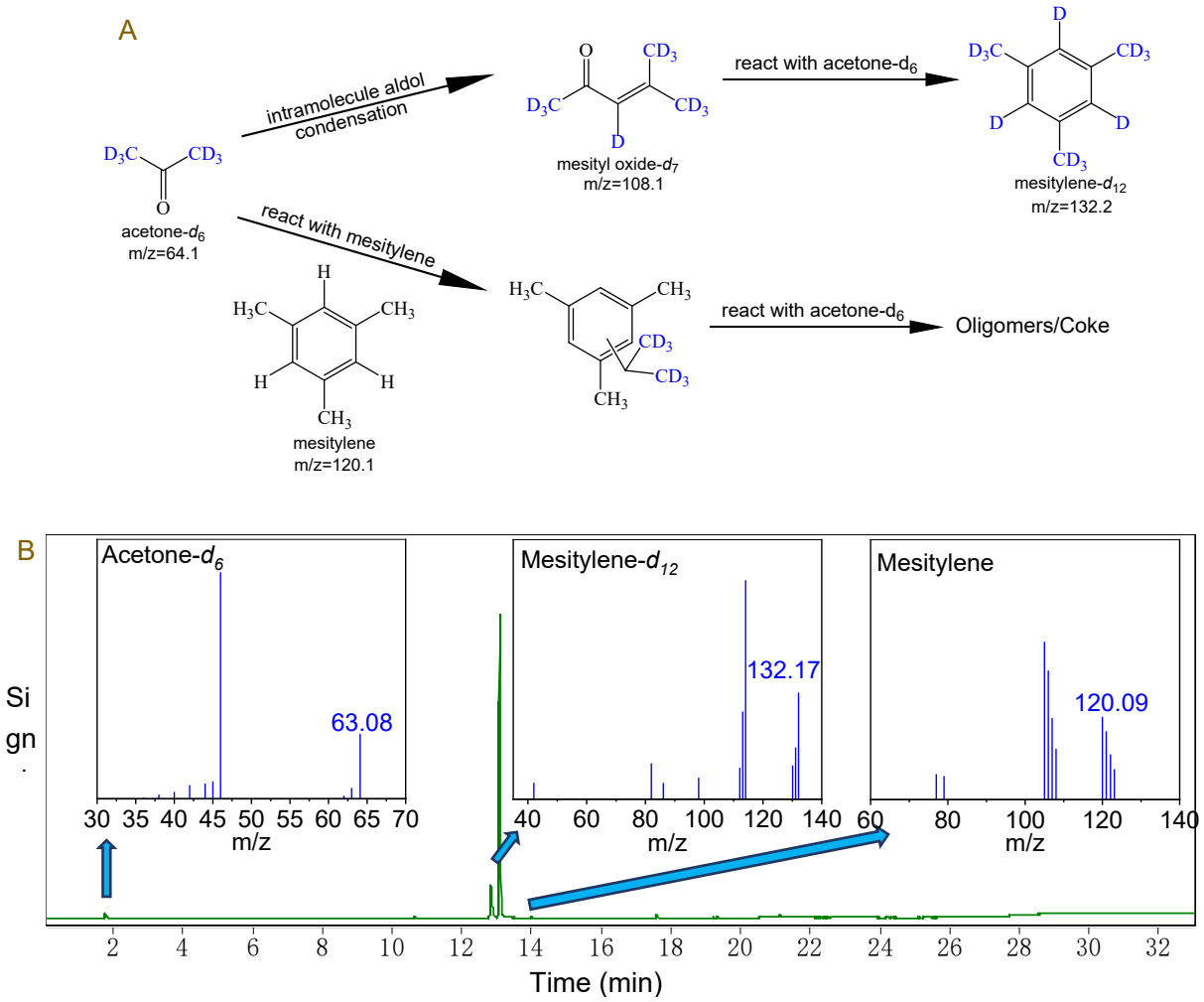

Figure S23. (A) Possible steps in the conversion of a mixture of acetone-d_6 and mesitylene; (B) GC-MS profile of the product over TaPO-1 catalyst in the conversion of the mixture of acetone-d_6 and mesitylene. Reaction conditions: 0.32 g of catalyst, mixture flow rate 0.6 ml/h, N_2 30mL/min, 200 °C, reaction for 1 h. Inserts in B are the MS profile of acetone-d_6, mesitylene, and mesitylene-d_{12}.

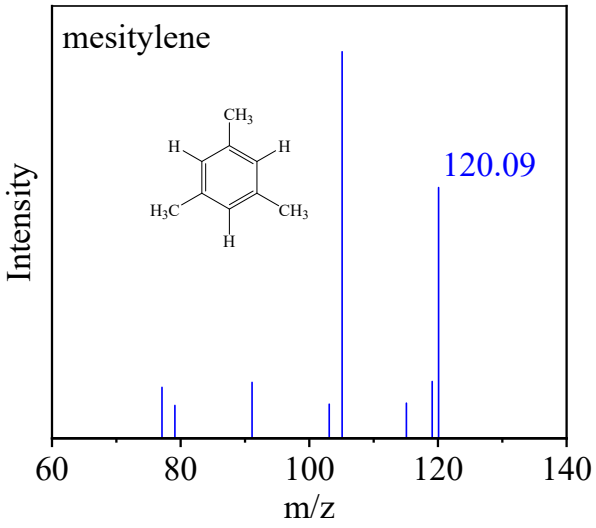

Figure S24. Mass spectrum of mesitylene.

Note: The m/z of the molecular ion peak of mesitylene is 120.09. However, the hydrogen-deuterium (H-D) exchange might occur when some deuterium-containing substrates were present. Therefore, part of the mesitylene might be transferred into deuterium-containing mesitylene. It is reasonable that the peaks with m/z at 121.0, 122.1, and 123.1 are present in the mass spectrum in Figure 4 in the main text.[10]

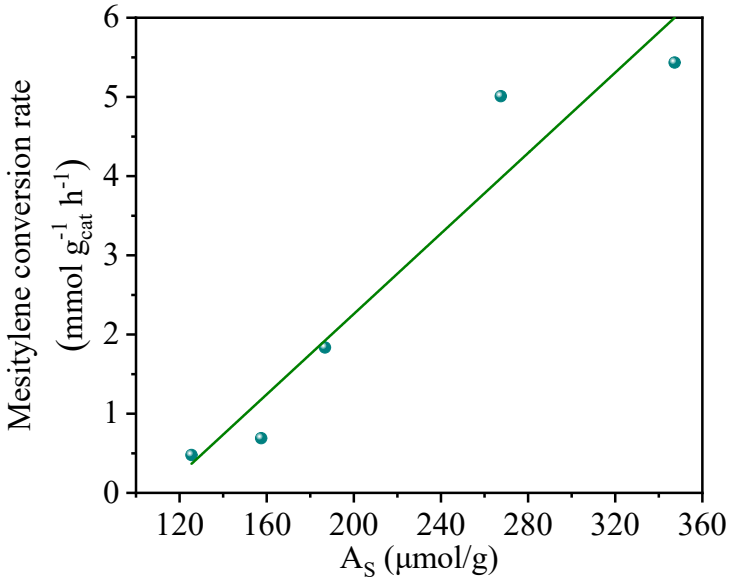

Figure S25. Mesitylene conversion rate as a function of strong acid (A_S) concentration over the TaPO-0.5, TaPO-1, TaPO-2, TaPO-3, and Ta_2O_5 samples.

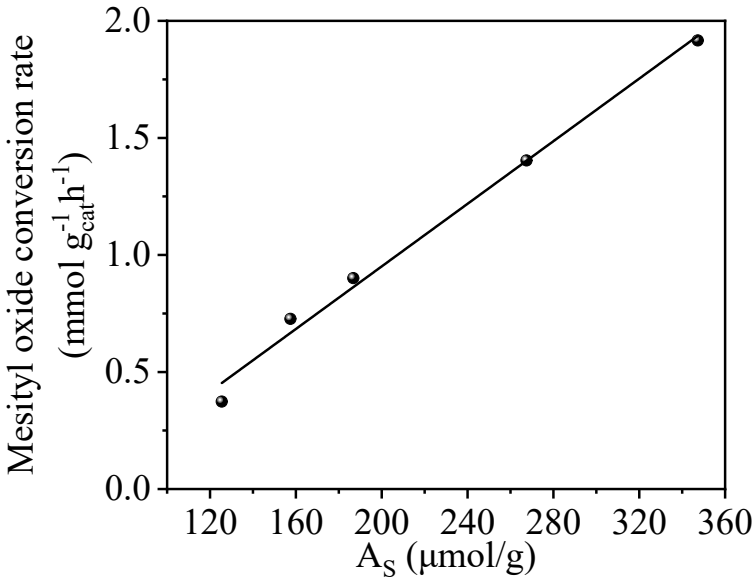

Figure S26. Mesityl oxide conversion rate as a function of strong acid (A_S) concentration over the TaPO-0.5, TaPO-1, TaPO-2, TaPO-3, and Ta_2O_5 samples in the conversion of mesityl oxide. Reaction conditions: WHSV at 1.10 h^{-1}, 9.3 vol % mesityl oxide in N_2, 200 °C.

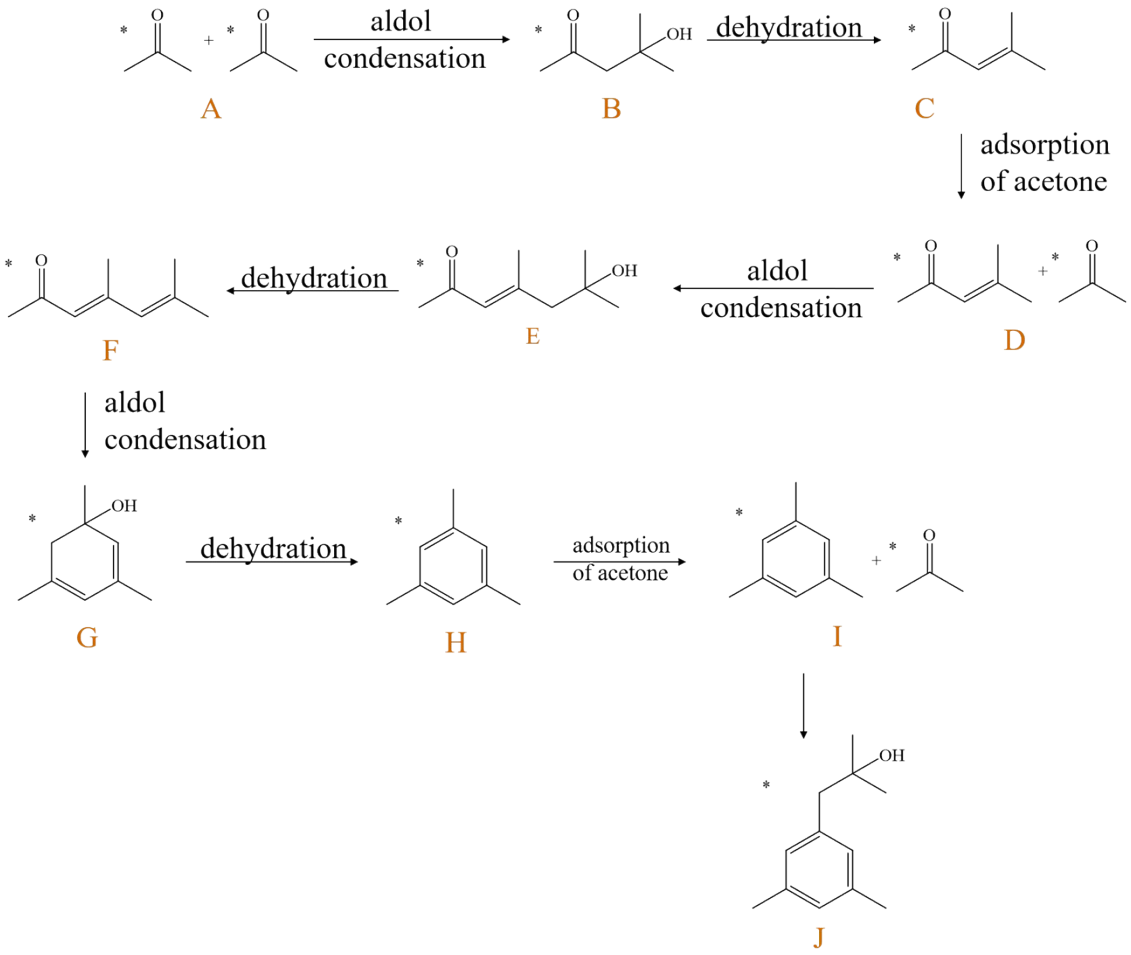

Figure S27. Proposed reaction process in the catalytic conversion of acetone to mesitylene. The structure formulas of each step are labelled by alphabet "A-J", which is in accordance with Figure 3 in the maintext.

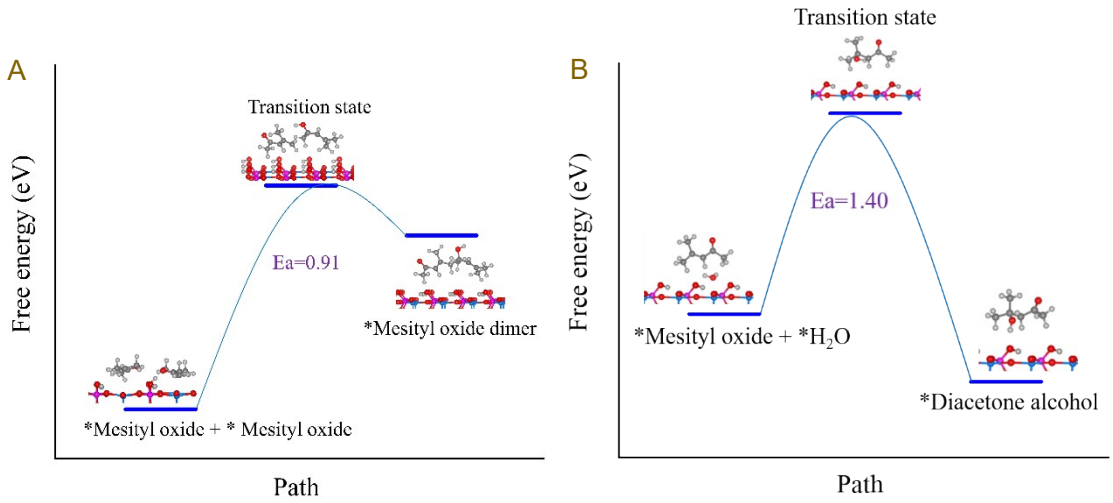

Figure S28. Calculated energies for mesityl oxide (A) hydration and (B) oligomerization on the TaPO-1 sample. The Ta, P, O, C, and H atoms are shown as blue, pink, red, gray, and light gray balls, respectively. Ea is the activation energy, and the energy difference of each step was given by blue number, respectively.

Note: Based on the experimental results, the intermediate in the catalytic conversion of acetone to mesitylene is mesityl oxide. Therefore, the reactions of mesityl oxide should also be considered in the computational studies. Mesityl oxide might oligomerize to form acetone tetramer, which would be finally transformed into oligomer/coke. The calculated results show that the activation barrier was 0.91 eV (Figure S28A), which is similar to the value by mesityl oxide reacting with acetone (Figure 3). Considering that the rate for converting acetone to mesityl oxide is faster based on both experimental and computational results, the concentration of mesityl oxide on the catalyst surface should be much lower than that of acetone during reaction, therefore it is suggested that mesityl oxide would preferentially react with acetone to form mesitylene.

Furthermore, mesityl oxide might rehydrate to form diacetone alcohol, and the activation barrier was 1.40 eV (Figure S28B), which is higher than that of aldol condensation step (react with acetone, 0.91 eV) and the oligomerisation step (0.91 eV). Therefore, the oligomerization of mesityl oxide might modify the catalyst activity during reaction.

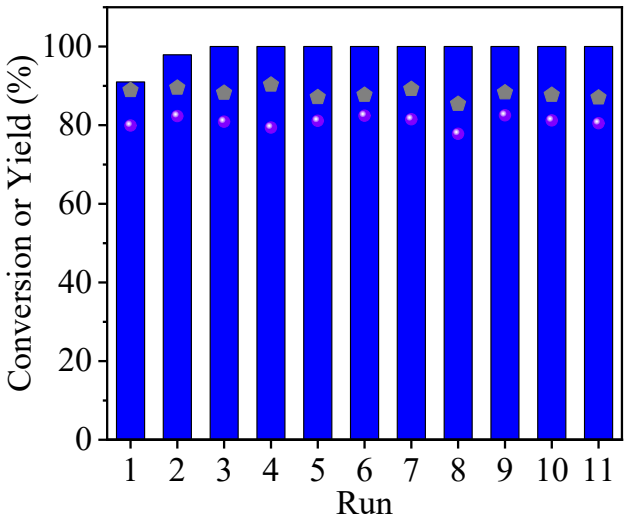

Figure S29. Conversion of acetone (blue colume), mesitylene yield (violet sphere), and carbon balance (grey pentagon) as a function of recycle time. The reaction conditions are the same as those in Figure 2. The spent catalyst was regenerated in flowing O_2 (30 mL/min) at 400 °C for the next run.

Note: Typically, the recyclable tests should be performed under reaction conditions with low substrate conversions. However, acetone is the only substrate in the catalytic conversion of acetone to mesitylene, high acetone conversion yield could be achieved with even higher acetone/catalyst ratio. But the products distributions were greatly influenced by the acetone/catalyst ratio, mesityl oxide was the major product with higher acetone/catalyst ratio. In order to study the catalytic ability for the production of mesitylene over the TaPO-1 catalyst, we performed the recyclable tests with the same conditions as those in Figure 2.

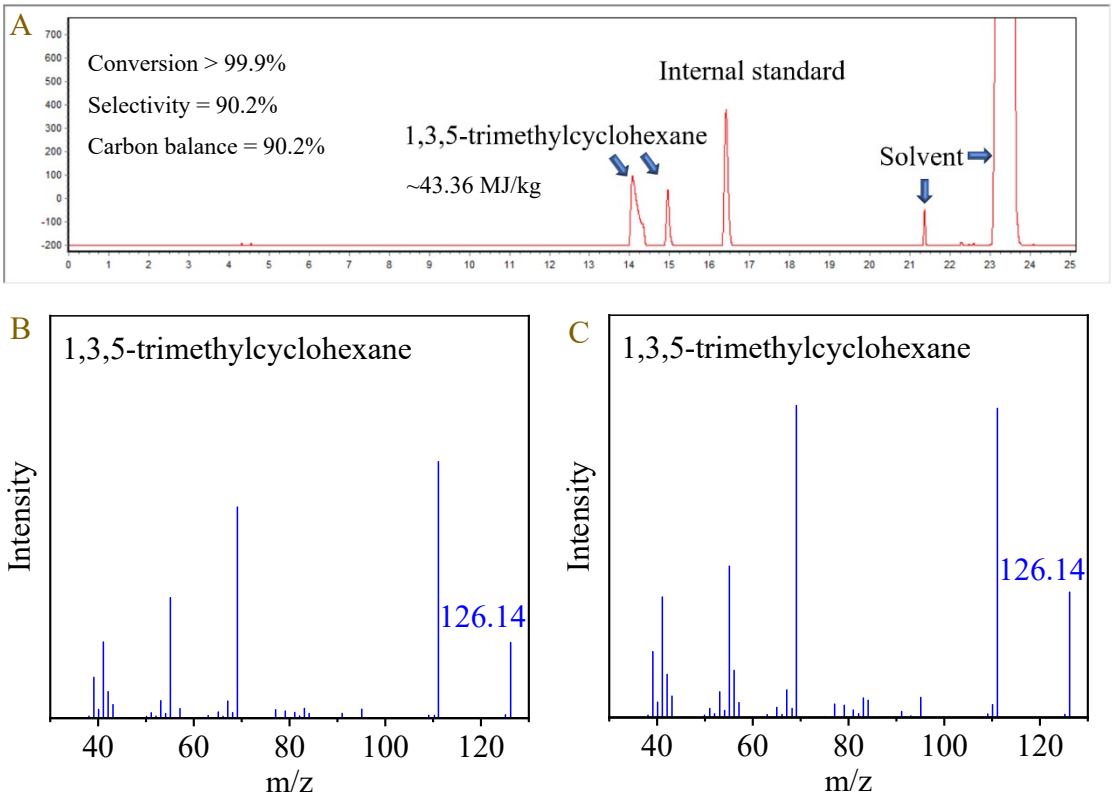

Figure S30. (A) GC profile of the product in the catalytic hydrogenation of mesitylene over 5% Pt/Al_2O_3 catalyst; (B and C) MS profile of the 1,3,5-trimethylcyclohexane. Reaction conditions: 5 mmol of mesitylene, 100 mg of 5% Pt/Al_2O_3 catalyst, 22 g of dodecane, 220 °C, 4 MPa of H_2, 4 h.

Note: 1,3,5-trimethylcyclohexane have two isomers, as shown in Figure S30.

Table S1. Textual parameters of various catalysts

Entry	Catalyst	S_{BET} (m^2/g)[a]	Vp (cm^3/g)[b]	Bulk P/Ta[c]	Surface P/Ta[d]
1	Ta_2O_5	36.5	0.084	-[e]	-[e]
2	TaPO-0.5	268.8	0.43	0.62	0.75
3	TaPO-1	314.1	0.43	0.90	1.05
4	TaPO-2	354.5	0.46	0.97	1.27
5	TaPO-3	174.3	0.35	1.12	1.41

[a] Calculated by BET

[b] Single point total pore volume at $P/P_0 = 0.993$

[c] Calculated basing on ICP analysis

[d] Calculated basing on XPS analysis

[e] Trace or undetectable

Table S2. Acid concentration of various catalysts.

Entry	Catalyst	Acid concentration (μmol/g)[a]						B/L[b]
		Weak acid (A_{wS}) concentration (μmol/g)[a]	Medium acid (A_M) concentration (μmol/g)[a]	Medium-strong acid (A_{MS}) concentration (μmol/g)[a]	Strong acid (A_S) concentration (μmol/g)[a]	Ultra-strong acid (A_{US}) concentration (μmol/g)[a]	Total strong acid (A_{MS}+ A_S+A_{US}) concentration (μmol/g)[a]	
1	TaPO-0.5	0	87.1	369.8	267.5	0	637.5	0.45
2	TaPO-1	0	0	111.3	157.5	637.3	906.1	1.17
3	TaPO-2	0	127.8	311.8	347.3	0	659.1	1.37
4	TaPO-3	500.6	683.3	101.9	125.5	118.6	346.0	2.19
5	Ta_2O_5	0	244.4	298.6	186.8	0	485.4	0
6	TiO_2	0	0	0	9.3	0	9.3	
7	Al_2O_3	0	63.5	134.8	167.7	0	302.5	

8	ZrO_2	0	0	3.9	14.8	0	18.7

[a] Determined by NH_3-TPD

[b] The ratio of Brønsted acid to Lewis acid, determined by Py-adsorption FT-IR

1 Q.-N. Xia, Q. Cuan, X.-H. Liu, X.-Q. Gong, G.-Z. Lu and Y.-Q. Wang, *Angew. Chem. Int. Ed.*, 2014, **53**, 9755-9760.

2 L. Dong, L. Lin, X. Han, X. Si, X. Liu, Y. Guo, F. Lu, S. Rudić, S. F. Parker, S. Yang and Y. Wang, *Chem* 2019, **5**, 1521-1536.

3 J. P. Perdew, K. Burke and M. Ernzerhof, *Phys. Rev. Lett*., 1996, **77**, 3865.

4 G. Kresse and D. Joubert, *Phys. Rev. B*, 1999, **59**, 1758.

5 D.J. Chadi, *Phys. Rev. B*, 1977, **16**, 5188-5192.

6 L. Gong, D. Zhang, C.Y. Lin, Y. Zhu, Y. Shen, J. Zhang, X. Han, L. Zhang and Z. Xia, *Adv. Energy Mater.*, 2019, **9**, 1902625.

7 J. K. Nørskov, T. Bligaard, A. Logadottir, J.R. Kitchin, J.G. Chen and S. Pandelov, *J. Electrochem. Soc.*, 2005, **152**, J23.

8 J. K. Nørskov, J. Rossmeisl, A. Logadottir, L. Lindqvist, J. R. Kitchin, T. Bligaard and H. Jónsson, *J. Chem. Phys. B*, 2004, **108**, 17886-17892.

9 L. I. Bendavid and E. A. Carter, *J. Phys. Chem. C*, 2013, **117**, 26048-26059.

10 Y. C. He, J. G. Pan, D. S. Liu, *Tetrahedron Lett.*, 2016, **57**, 3133-3136.